Received: 24 June 2020 | Revised: 7 December 2020 | Accepted: 8 December 2020

DOI: 10.1111/joa.13388

Journal of Anatomy ANATOMICAL SOCIETY WILEY

ORIGINAL PAPER

Keratan sulfate as a marker for medullary bone in fossil vertebrates

Aurore Canoville[1,2] | Lindsay E. Zanno[1,2] | Wenxia Zheng[2] | Mary H. Schweitzer[1,2]

[1]Paleontology, North Carolina Museum of Natural Sciences, Raleigh, NC, USA

[2]Department of Biological Sciences, North Carolina State University, Raleigh, NC, USA

Correspondence
Aurore Canoville, Paleontology, North Carolina Museum of Natural Sciences, Raleigh, NC, USA.
Email: canoville.aurore08@gmail.com

Funding information
National Science Foundation, Grant/Award Number: 1552328

Abstract

The ability to determine the sex of extinct dinosaurs by examining the bones they leave behind would revolutionize our understanding of their paleobiology; however, to date, definitive sex-specific skeletal traits remain elusive or controversial. Although living dinosaurs (i.e., extant birds) exhibit a sex-specific tissue called medullary bone that is unique to females, the confident identification of this tissue in non-avian archosaurs has proven a challenge. Tracing the evolution of medullary bone is complicated by existing variation of medullary bone tissues in living species; hypotheses that medullary bone structure or chemistry varied during its evolution; and a lack of studies aimed at distinguishing medullary bone from other types of endosteal tissues with which it shares microstructural and developmental characteristics, such as pathological tissues. A recent study attempted to capitalize on the molecular signature of medullary bone, which, in living birds, contains specific markers such as the sulfated glycosaminoglycan keratan sulfate, to support the proposed identification of medullary bone of a non-avian dinosaur specimen (*Tyrannosaurus rex* MOR 1125). Purported medullary bone samples of MOR 1125 reacted positively to histochemical analyses and the single pathological control tested (avian osteopetrosis) did not, suggesting the presence of keratan sulfate might serve to definitively discriminate these tissues for future studies. To further test these results, we sampled 20 avian bone pathologies of various etiologies (18 species), and several MB samples. Our new data universally support keratan sulfate as a reliable marker of medullary bone in birds. However, we also find that reactivity varies among pathological bone tissues, with reactivity in some pathologies indistinguishable from MB. In the current sample, some pathologies comprised of chondroid bone (often a major constituent of skeletal pathologies and developing fracture calluses in vertebrates) contain keratan sulfate. We note that beyond chemistry, chondroid bone shares many characteristics with medullary bone (fibrous matrix, numerous and large cell lacunae, potential endosteal origin, trabecular architecture) and medullary bone has even been considered by some to be a type of chondroid bone. Our results suggest that the presence of keratan sulfate is not exclusive evidence for MB, but rather must be used as one in a suite of criteria available for identifying medullary bone (and thus gravid females) in non-avian dinosaur specimens. Future studies should investigate whether there are definite chemical or

microstructural differences between medullary bone and reactive chondroid bone that can discriminate these tissues.

KEYWORDS
chondroid bone, dinosaur reproduction, immunogold, avian reproduction, skeletal pathologies

1 | INTRODUCTION

The ability to determine biological sex would revolutionize our understanding of the evolution and ecology of extinct dinosaurs (e.g., Lee & Werning, 2008; Persons et al., 2015; Saitta, 2015; Varricchio et al., 2008; Woodward et al., 2015). Although features exist that have been hypothesized to be linked to sex in extinct dinosaurs, for the most part these cannot be tested against rigorous identifications of male and female morphs because such evidence is elusive or contested (see discussions in Barden & Maidment, 2011; Canoville et al., 2020a; Chapman et al., 1997; Erickson et al., 2005; Mallon, 2017; Padian & Horner, 2011, 2014). Indeed, to date, the only definitive exemplars of female dinosaurs derive from specimens that include ichnological or soft tissue evidence of biological sex, including two reported cases of oviraptosaurian dinosaurs that died with eggs in the body cavity (Jin et al., 2020; Sato et al., 2005) and avialan specimens bearing maturing ovarian follicles or eggshell material (Bailleul et al., 2019; Zheng et al., 2013). Given the rarity of such preservation, robust skeletal indicators of biological sex are needed to advance our understanding of dinosaurian reproductive biology.

The presence of medullary bone in various dinosaur lineages has been touted as a potential skeletal indicator of biological sex. Medullary bone is an ephemeral, labile, sex-specific bone tissue deposited within the skeleton of living dinosaurs (birds) that is unique to gravid females and greatly contributes to the calcium supply required for eggshell deposition (Dacke et al., 1993). The structure and composition of this tissue has been widely investigated in commercial egg-layers, because of its importance in offsetting osteoporosis during the egg-laying cycle. These studies have shown that, in addition to an endosteal origin and a woven-fibered lattice, the matrix of medullary bone presents unique chemical properties that distinguish it from the surrounding cortical and trabecular bone tissues, and correlate to the rapid turnover required of this tissue. As a result, medullary bone comprises proportionally less collagen fibers than structural bone, but instead has abundant non-collagenous proteins and sulfated proteoglycans. Rather than chondroitin sulfate (the predominant glycosaminoglycan in cortical and trabecular bone) medullary bone incorporates keratan sulfate. This glycosaminoglycan persists in the calcified matrix of medullary bone and is thus broadly recognized as one of its specific markers (Candlish & Holt, 1971; Fisher & Schraer, 1982; Hadley et al., 2016; Schweitzer et al., 2016; Yamamoto et al., 2005). Because of its abundance and acidity, the presence of this glycosaminoglycan can be detected with chemical stains, such as high iron diamine (HID) and Alcian blue. These dyes react preferentially and intensely with keratan sulfate in the matrix of medullary bone, but only lightly stain the surrounding structural bone matrix (Bonucci & Gherardi, 1975; Candlish & Holt, 1971; Spicer, 1965; Yamamoto et al., 2001, 2005). In addition to stains, monoclonal antibodies raised against keratan sulfate have been used to study the distribution of this component in medullary bone with clear specificity (e.g., Schweitzer et al., 2016; Yamamoto et al., 2005).

Although the existence of medullary bone-like tissues has been proposed for various lineages of non-avian dinosaurs based on location and microstructure (Cerda & Pol, 2013; Chinsamy et al., 2016; Hübner, 2012; Lee & Werning, 2008; Skutschas et al., 2017), some avian pathological bone tissues have been shown to share microstructural (highly vascularized and woven-like matrix) and origin (endosteal) characteristics with avian MB, casting doubts on previous identifications of purported medullary bone-like tissues in the fossil record (i.e., Canoville et al., 2020a; Chinsamy et al., 2016; Chinsamy & Tumarkin-Deratzian, 2009; Prondvai, 2017). To address this issue, a single study (Schweitzer et al., 2016) applied histochemical analyses to a non-avian dinosaur specimen (i.e. *Tyrannosaurus rex* MOR 1125), to ascertain the chemical nature of medullary bone-like tissues previously observed in its femur (Schweitzer et al., 2005). Results of these chemical analyses were positive when compared to similar tests on medullary bone in two extant birds (a laying hen and an ostrich) that died during the laying cycle. As a control, Schweitzer et al. (2016) also tested the hypothesis that medullary bone is chemically distinct from avian skeletal pathologies, by including in the analyses a single sample of osteopetrotic tissue, a virally induced reactive bone lesion (Banes & Smith, 1977), from the tarsometatarsus of an infected chicken (see Schweitzer et al., 2016 – Supplementary Material). They found no evidence that this pathological tissue reacted with stains or antibodies that yielded a positive response for medullary bone. This suggested that osteopetrotic bone matrix lacked the keratan sulfate marker consistent with medullary bone in extant birds and *T. rex* (MOR 1125) and moreover, raised the possibility that the presence of keratan sulfate could serve as a single, standalone criterion for eliminating alternative hypotheses of pathology for enigmatic endosteal tissues in fossil specimens. However, it is reasonable to hypothesize that different skeletal pathologies that show variable microstructures, etiologies (e.g., fracture, infection, cancer), or developmental stages (developing vs. mature lesions), could have different molecular compositions. To date, the methodologies used by Schweitzer et al. (2016) to rule out a potential pathological origin for purported medullary bone tissues in extinct dinosaurs have not been tested against other avian pathologies.

To more rigorously test the hypothesis that keratan sulfate can reliably be used to identify medullary bone (and thus mature female

individuals) in the fossil record and reject the hypothesis of a pathological origin, we increased the number and types of avian pathologies used as controls, subjecting a sample of 20 randomly selected avian skeletal pathologies (of varying etiologies and exhibiting different external morphologies), across 18 wild bird species (Table S1) to histochemical staining and immunological tests.

2 | MATERIALS AND METHODS

2.1 | Biological sample

We randomly screened for avian skeletal pathologies in the osteological collections of the Ornithology Unit of the North Carolina Museum of Natural Sciences (NCSM), Raleigh NC, USA. We identified grossly diverse skeletal pathologies, of different etiology (including both fracture calluses and infectious lesions; see Table S1 and Figures S1-S19) in 20 specimens representing 18 bird species (and comprising six major bird clades: Anseriformes, Aequorlitornithes, Accipitriformes, Falconiformes, Psittaciformes, Passeriformes; Prum et al., 2015). We also re-analyzed the same osteopetrotic tarsometatarsus of the female *Gallus gallus* previously studied by Schweitzer et al. (2016). Finally, as positive controls, we included four female birds that died during the egg-laying cycle and possessed medullary bone in at least some skeletal elements (Table S1).

2.2 | Terminology of skeletal tissues under consideration

In this study, the authors follow the histological terminology on Francillon-Vieillot et al. (1990), Witten et al. (2010), and Hall (2015). The skeletal tissues under investigation encompass avian medullary bone, avian cortical and trabecular bones, and different types of avian bone pathologies. As described in previous studies, avian skeletal pathologies can comprise a mix of tissues, including calcified cartilage, woven bone, and tissues pertaining to the chondroid bone spectrum (e.g., Beresford, 1981; Franch et al., 1998; Nyssen-Behets et al., 1988). This last group of tissues is of particular interest for our study and deserves some brief definition. Tissues belonging to the chondroid bone spectrum are described in the literature as permanent tissues, distinct from cartilage and bone but with characteristics intermediate between them (Beresford, 1981; Fang & Hall, 1997; Hall, 2015). Chondroid bone usually contains chondrocyte-like cells/lacunae that are larger than the static osteocytes (lacunae) of woven bone, generally organized in clusters, and with short or no cell processes (i.e., canaliculi; Hall, 2015; Prondvai et al., 2020; Witten et al., 2010). Despite their chondrocyte-like morphology, these cells partly assume an osteoblastic activity (e.g., Hall, 2015; Witten et al., 2010). The extracellular matrix of chondroid bone can be vascularized (unlike most cartilage types; Hall, 2015), its degree of mineralization and histology are similar to rapidly deposited woven bone. Although the matrix of chondroid bone is dominated by collagen I, as other bone types, it also contains cartilage-specific collagen II in the pericellular regions (Fang & Hall, 1997; Goret-Nicaise, 1984; Goret-Nicaise & Dhem, 1987; Hall, 2015). Chondroid bone can either form via intramembranous ossification, without any cartilaginous precursor, or via endochondral ossification (Hall, 2015). Finally, chondroid bone can have a periosteal or an endosteal origin (Nyssen-Behets et al., 1988).

2.3 | Micro-CT scanning and candling

To ascertain that our pathological specimens did not contain medullary bone, and to assess the skeletal distribution of the sampled pathologies (and their periosteal and/or endosteal development; Table S1), we used micro-computed tomography (CT) to scan the (sub-) complete skeletons of most females and some specimens for which the sex had not been recorded in the collection database (see Table S1) with a high-resolution microCT scanner (Nikon XTH 225 ST) at the Shared Materials Instrumentation Facility of the Duke University, Durham NC, USA. Data were imported into Avizo Lite (version 9.0.0) for visualization. None of the micro-CT-scanned pathological specimens exhibited MB, based on known criteria pertaining to the skeletal distribution of this tissue (see Canoville et al., 2019). All micro-CT data produced for this study are available in the MorphoSource repository, under the project P1053 at https://www.morphosource.org (Canoville et al., 2020b). The limb elements of female specimens that could not be subjected to micro-CT scanning were candled following the technique described in Werning (2018). The candling results are also recorded in Table S1.

2.4 | Petrographic ground sections

We processed ground-sections for all sampled NCSM pathological specimens following standard petrographic protocols (Lamm, 2013) in the Paleontology Research Lab of the North Carolina Museum of Natural Sciences, Raleigh, NC. The bone fragments were dehydrated in progressive alcohol baths (70%–100%), defatted in acetone, and embedded in a clear polyester casting resin (EPO-TEK 301). A slice of embedded bone was cut with a Buehler IsoMet 1000 Precision Saw, affixed to a glass slide with epoxy, and ground to desired thickness (100 – 80 μm) with a Buehler MetaServ 250 Grinder-Polisher. Ground-sections were observed with a Nikon Eclipse C*i* POL microscope and imaged with a Nikon DS-Fi2 digital camera (see Figures S1-S19).

2.5 | Paraffin thin sections and chemical staining

All 20 pathological specimens and four medullary bone specimens (controls) were subjected to additional testing by staining with Alcian blue, HID, and standard hematoxylin/eosin, following the protocols detailed in Schweitzer et al. (2016) to test for the presence

and distribution of keratan sulfate in the different tissues. Although Alcian blue and HID can react with other sulfated glycosaminoglycans incorporated into various cartilaginous and bone matrices (Page & Ashhurst, 1987; Schumacher & Adam, 1994) these stains have been used to diagnose medullary bone (due to its characteristic chemical composition that includes large amounts of sulfated glycosaminoglycans and thus an acidic extracellular bone matrix) and discriminate between medullary bone and surrounding cortical and trabecular bone based on their different chemistries (Bonucci & Gherardi, 1975; Candlish & Holt, 1971; Spicer, 1965; Yamamoto et al., 2001, 2005).

Bone samples were fixed with neutral buffered 10% formalin overnight, then demineralized in 500 mM EDTA (pH 8.0) until all mineral was removed, as evidenced by the flexibility of the tissues, and again subjected to fixation as above. Demineralized samples were then subjected to dehydration (via sequential incubations in 70%, 80%, 90%, 95%, and 100% alcohols for ~1 h each), followed by three, 30-min incubations in 100% xylene to clear the tissues. Tissues were then transferred to three separate and sequential incubations in 100% paraffin for 30 min each, to complete infiltration, and finally, embedded in paraffin wax (Paraplast Plus EMS) for sectioning. Sections were taken at 5 μm, using a Leica RM 2255 microtome. Paraffin-embedded sections were deparaffinized with xylene, and dehydrated through a graded ethanol series. The demineralized bone sections were either stained with Alcian blue (8GX used as follow: 1% in 3% acetic acid, at 2.5 pH) for 30 min, or oxidized in 1% periodic acid for 10 min, rinsed under running tap water, then incubated with freshly made HID solution overnight. Sections were then rinsed with tap water, dehydrated with a graded ethanol series, followed by three incubations in 100% xylene, and mounted with a mounting medium (Poly-Mount, PolySciences) and cover glass for visualization. Paraffin sections were examined with a Zeiss Axioskop 2 microscope and imaged using an AxioCam MRc 5 (Zeiss) digital camera and the Axiovision software package (version 4.7.0.0). All paraffin sections and chemical staining analyses were conducted in the modern tissue section of the Molecular Paleontology laboratory of the Biological Sciences Department, North Carolina State University, Raleigh, NC, USA.

2.6 | Immunohistochemistry

A subsample of demineralized pathological and medullary bone specimens (see Table S2) was subjected to immunohistochemical analyses. The samples were first fixed in 10% neutral buffered formalin, then washed three times with 1X phosphate buffered saline (PBS). Sections were, dehydrated in 2 changes of 70% ethanol for 30 min each, followed by 1 h incubation in LR white: 70% ethanol (2:1). Samples were then incubated in 3 changes of undiluted LR white for 1 h each, then embedded and polymerized for 24 h at 60°C. A Leica EMUC6 ultra-microtome with a Diatome 45° knife was used to cut 200 nm and/or 90 nm sections for immunofluorescence and/or immunogold labeling, respectively (see below). The ultrathin-sections were transferred to Teflon-coated slides, and dried overnight at 45°C on a warming plate before further analyses.

2.6.1 | Immunofluorescence with anti-keratan sulfate antibodies

We used specific antibodies to test for the presence of the keratan sulfate in the organic matrix of selected pathological and MB specimens, because this glycosaminoglycan dominates in medullary bone, but not in cortical or trabecular tissues (Candlish & Holt, 1971; Fisher & Schraer, 1982; Hadley et al., 2016; Yamamoto et al., 2005). Sections were taken as described above, then etched with Proteinase K (PCR grade, Roche, 25 μg/ml) in 1X phosphate buffered saline (PBS) buffer at 37°C to expose epitopes, followed by two incubations in 500 mM EDTA (pH 8.0) and two incubations in 1 mg/ml sodium borohydride for 10 min each for antigen retrieval (http://www.ihcworld.com/_intro/antigen-retrieval.htm) and reduction of autofluorescence. Sections were then incubated for 2 h in normal goat serum (NGS) diluted to 4% in PBS to occupy nonspecific binding sites and prevent spurious binding. This was followed by another incubation with monoclonal mouse anti-keratan sulfate [Keratan Sulfate (5D4) antibodies, previously used to detect keratan sulfate in medullary bone (Schweitzer et al., 2016; Yamamoto et al., 2005) or other tissue types (i.e., Page & Ashhurst, 1987)] (Cosmo Bio Co., LTD Cat no. PRPG-BC-M01), diluted 1:20 in primary dilution buffer overnight at 4°C as recommended by the manufacturer. Sections were washed multiple times to remove unbound antibody, then all sections, including controls (no primary antibodies were applied but all other steps and conditions were kept identical), were then incubated with secondary antibody (biotinylated goat anti-mouse IgG (H + L) (Vector BA-9200), diluted 1:500 in antibody dilution buffer 12 for 2 h at room temperature. Fluorescein Avidin D (FITC, Vector Laboratories A-2001) diluted 1:1000, was applied to all sections and allowed to bind for 1 h at RT. All incubations were separated by sequential washes (2 times for 10 min each) in PBS w/ Tween 20 (ACROS Organics) followed by two 10 min rinses in PBS. Finally, sections were mounted with Vectashield Anti-Fade mounting medium (Vector H-1000), and coverslips applied. Sections were examined with a Zeiss Axioskop 2 plus biological microscope and captured using an AxioCam MRc 5 (Zeiss) with 10× ocular magnification, and data collected using the Axiovision software package (version 4.7.0.0).

2.6.2 | Immunofluorescence with anti-type I collagen antibodies

To ensure that anti-keratan sulfate antibodies were binding to medullary bone and not the surrounding cortical bone we subjected our gravid bird samples to anti-type I collagen antibodies. This protocol also allowed us to ensure our pathological tissues were composed of a bone-type matrix (mostly containing type I collagen) and not cartilage,

which would mostly contain type II collagen. We followed the same protocol as above, but used a polyclonal rabbit anti-chicken collagen type I (US Biological C7510-13B) as our primary antibody, diluted 1:75 in primary dilution buffer. The secondary antibody consisted of biotinylated goat anti-rabbit IgG.

2.6.3 | Immunogold labeling and TEM observations

We complemented our immunofluorescence analyses with immunogold labeling for a few selected specimens (see Table S2). Immunogold labeling allows identification of antibody-antigen complexes at very high resolution and ensures that the anti-keratan sulfate binding observed in these specimens is tissue-specific. The post-embedding immunogold labeling protocol was modified from the method shared in the protocol database at IHCWORLD- Life Science Products and Sciences at http://www.ihcworld.com/_protocols/em/post_immunoem_l.r.white.htm. Briefly, 90 nm sections were collected on carbon-coated nickel grids (EMS Cat CFT200-NI), and incubated on droplets of PBS-Tween 20 for 10 min. 4% Normal Donkey serum (NDS) was applied to occupy non-specific binding sites and prevent spurious binding, and allowed to incubate for 1 h at room temperature. Sections on grids were then incubated with primary antibody (Monoclonal Mouse anti-Keratan Sulfate 5D4; Cosmo Bio Co LTD Cat no. PRPG-BC-M01) 1:4) in primary dilution buffer (1% Bovine Serum Albumin (BSA) (Fisher, BP1660-100), 0.1% Cold Fish Skin Gelatin (Sigma G7765), 0.05% Sodium Azide (sigma S-8032), 0.01 M PBS pH 7.2) for 3 h at room temperature. Sections were rinsed with TBS-Tween for 10 × 2 min. All grids were then incubated with secondary antibodies (12 nm Colloidal Gold AffiniPure Donkey Anti-Mouse IgG (H + L) 1:20 (Jackson Immuno Research Inc Cat 715-205-150) in Secondary dilution buffer (0.01 M PBS, pH 7.2; 0.05% Tween 20) for 1 h. The grids were rinsed with PBS-Tween20 for 10 × 2 min, in pure water 3 × 30 sec and dried with filter paper. Sections were stained with 5% methanolic uranyl acetate for 5 min and Reynold's lead citrate for 8 min. The sections were then observed using the Talos F200X G2 electron microscope of the Analytical Instrumentation Facility (AIF) of the North Carolina State University, Raleigh NC, USA.

3 | RESULTS

3.1 | Medullary bone specimens

3.1.1 | Microstructure

Our medullary bone samples exhibited the common microstructure known in Neognathes, that is, a highly vascular, spiculated trabecular-like tissue, comprising a mostly disorganized and woven matrix resulting in isotropy. Plump osteocytes were abundant and easily visualized within this matrix (Canoville et al., 2020a; Dacke et al., 1993; Simkiss, 1961).

3.1.2 | Histochemical staining

High iron-diamide and Alcian blue were applied to all medullary bone specimens as a positive control. These stains reacted as expected preferentially with the medullary bone matrix, but not with the surrounding cortical bone tissue (see Figure 1). Thus, medullary bone appears blue (Alcian blue staining) or dark pink (HID staining) and contrasts with the adjacent endosteal (internal circumferential layer; see Mitchell et al., 2017) and periosteal cortical bone tissues that remain unstained.

3.1.3 | Immunofluorescence

In all medullary bone specimens tested, monoclonal antibodies specific to keratan sulfate showed binding to demineralized medullary bone matrix, but not to the associated cortical bone tissue (Figure 3a, b, e, and f). As a control, antibodies specific to type I collagen were used and exhibited positive binding to both medullary bone and cortical bone tissues (Figure 3c, d, g, and h). These results highlight that anti-keratan sulfate antibodies capitalized on the chemical differences between medullary bone and cortical bone, and were specifically binding to medullary bone matrix, not the surrounding cortical bone matrix.

3.1.4 | Ultrastructural observations (with TEM) and immunogold labeling

As controls, we submitted the limb elements of three female birds containing medullary bone to TEM observations and immunogold labeling with anti-keratan sulfate antibodies (Table S2). For all three specimens, the cortical bone tissue showed a similar ultrastructure with densely packed collagen fibers and negative binding (Figure 4a-c, g-i). The medullary bone matrix, however, exhibited a very different ultrastructure than the associated cortical bone, with loosely packed collagen fibers and an overall spongiose organization. All tested specimens showed relatively high concentrations of antibody-antigen complexes revealed by the presence of electron-dense gold beads in the medullary bone matrix but not the surrounding cortical bone or embedding medium (LR white; see Figure 4).

3.2 | Sampled skeletal pathologies

3.2.1 | Skeletal distribution, microstructure, and possible etiology

The sampled pathologies present different skeletal distributions and microstructures, in keeping with their different etiologies (see Table S1). Gross-anatomical observations, as well as CT-data, reveal that some bone pathologies are restricted to a single skeletal element or closely associated bones as expected for fracture calluses and

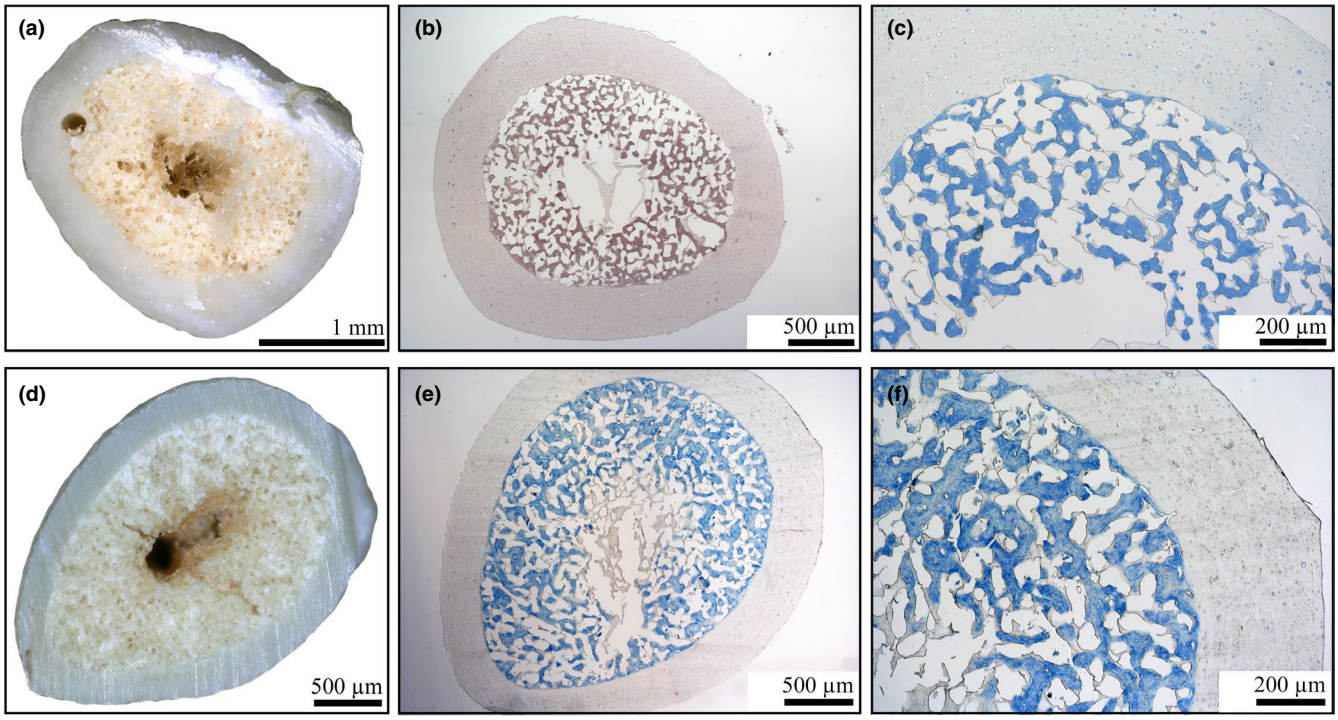

FIGURE 1 Microstructure and histochemical staining of two bird specimens, NCSM 13934 *Callipepla gambelii* tibiotarsus (a-c) and USNM 635083 *Anas cyanoptera* femur (d-f), showing medullary bone. (a) Hand sample in cross section; (b) demineralized paraffin cross section stained with HID; (c) demineralized paraffin cross-section stained with Alcian Blue; (d) hand sample in cross section; (e and f) demineralized paraffin cross-section stained with Alcian Blue

illustrated by NCSM 19439 *Corvus ossifragus*, in which the fracture affected the associated radius and ulna (see Figure S1). Other pathologies are systemic in nature, with diagnostic features distributed among several skeletal elements with or without articulation, as in NCSM 10210, *Larus delawarensis*. Here, reactive pathological tissues are seen on the proximal head of the humerus and the associated scapula and coracoid (see CT-data in MorphoSource Project P1053; Canoville et al., 2020b). These pathological tissues cannot be directly linked to fracture, and their etiology remains uncertain (Table S1).

Medullary bone is derived from the endosteal surfaces only, but most bone pathologies we observed show reactive tissues on both endosteal and periosteal surfaces (Table S1; Figure 2; Figures S1-S19), appearing, in most cases, simultaneously at a given position along the bone length. However, their distributions can be decoupled in a few areas (see NCSM 18761 *Ardea alba*, Figure 2g and Figure S19).

The reactive pathological tissues are, for the most part, comprised of highly vascularized, trabecular-like scaffolds that combine woven bone and tissues pertaining to the chondroid bone spectrum (see Figure 2). Some specimens exhibiting relatively older and more mature pathologies also exhibit deposition of parallel-fibered to lamellar bone tissues along the trabeculae of initial woven and/or chondroid tissues, or in the form of secondary osteons (Figure S20g,h).

In a few specimens, secondary cartilage (arising from the periosteum) was present (see strong blue and purple staining on Figure 2m-o), consistent with biomechanically unstable fracture healing sites (Beresford, 1981; Glimcher et al., 1980; Goret-Nicaise & Dhem, 1987; Fang & Hall, 1997; Page & Ashhurst, 1987; Page et al., 1986; Street et al., 2002). This tissue was easily distinguishable from the adjacent woven and chondroid pathological bone tissues. Secondary cartilage is recognized by poorly-vascularized areas, or areas containing completely avascular nodules, with proportionally lower amounts of extracellular matrix than the adjacent woven and chondroid bone tissues, but with numerous hypertrophic chondrocytes, which are much larger than bone cells (see Figure 2m-o; Figure S20i,j). Moreover, the matrix of secondary cartilage always reacted differently with the stains than the surrounding pathological woven and chondroid bone tissues. In demineralized sections exposed to Alcian blue and HID stains, as well as standard hematoxylin

FIGURE 2 Microstructure and histochemical staining of bone pathologies in five selected bird specimens: NCSM 10210 *Larus delawarensis* coracoid (a-c); NCSM 17977 *Cacatua moluccensis* radius (d and f); NCSM 18761 Ardea alba tarsometatarsus (g-i); NCSM 18795 Anser caerulescens radius (j-l); NCSM 17801 Stercorarius longicaud*us* pedal phalanx (m-o). (a, d, e, g, and j) Petrographic cross-sections; (b, f, h, and k-n) demineralized paraffin cross sections stained with Alcian Blue; (c) demineralized paraffin cross-section stained with HID. Note that HID and alcian blue stain preferentially the endosteal and/or periosteal pathological tissues as compared to the adjacent cortical bone. (o) Demineralized paraffin cross-section stained with hematoxylin and eosin. Note that the calcified cartilage stains purple

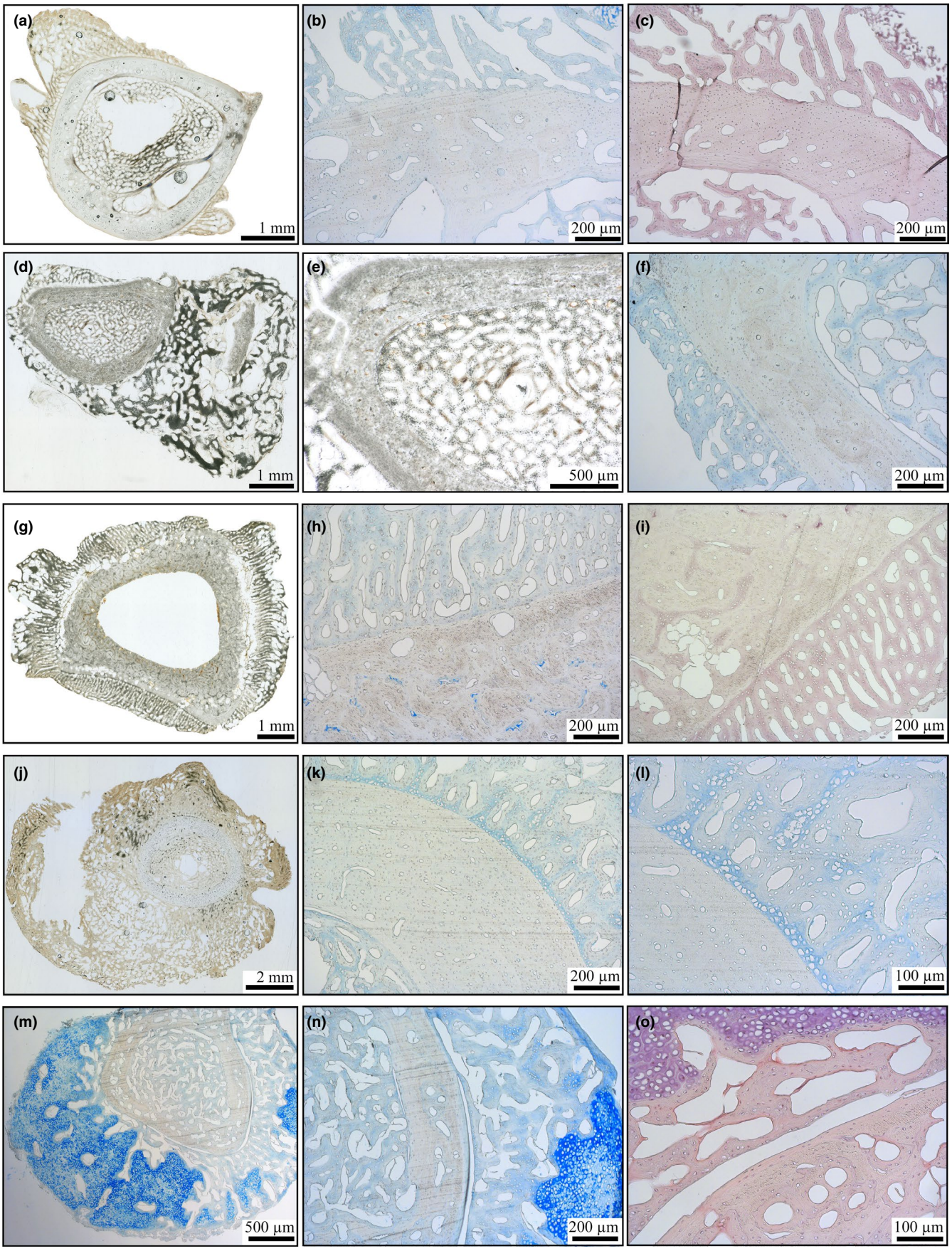
(a)
1 mm
(b)
200 µm
(c)
200 µm
(d)
1 mm
(e)
500 µm
(f)
200 µm
(g)
1 mm
(h)
200 µm
(i)
200 µm
(j)
2 mm
(k)
200 µm
(l)
100 µm
(m)
500 µm
(n)
200 µm
(o)
100 µm

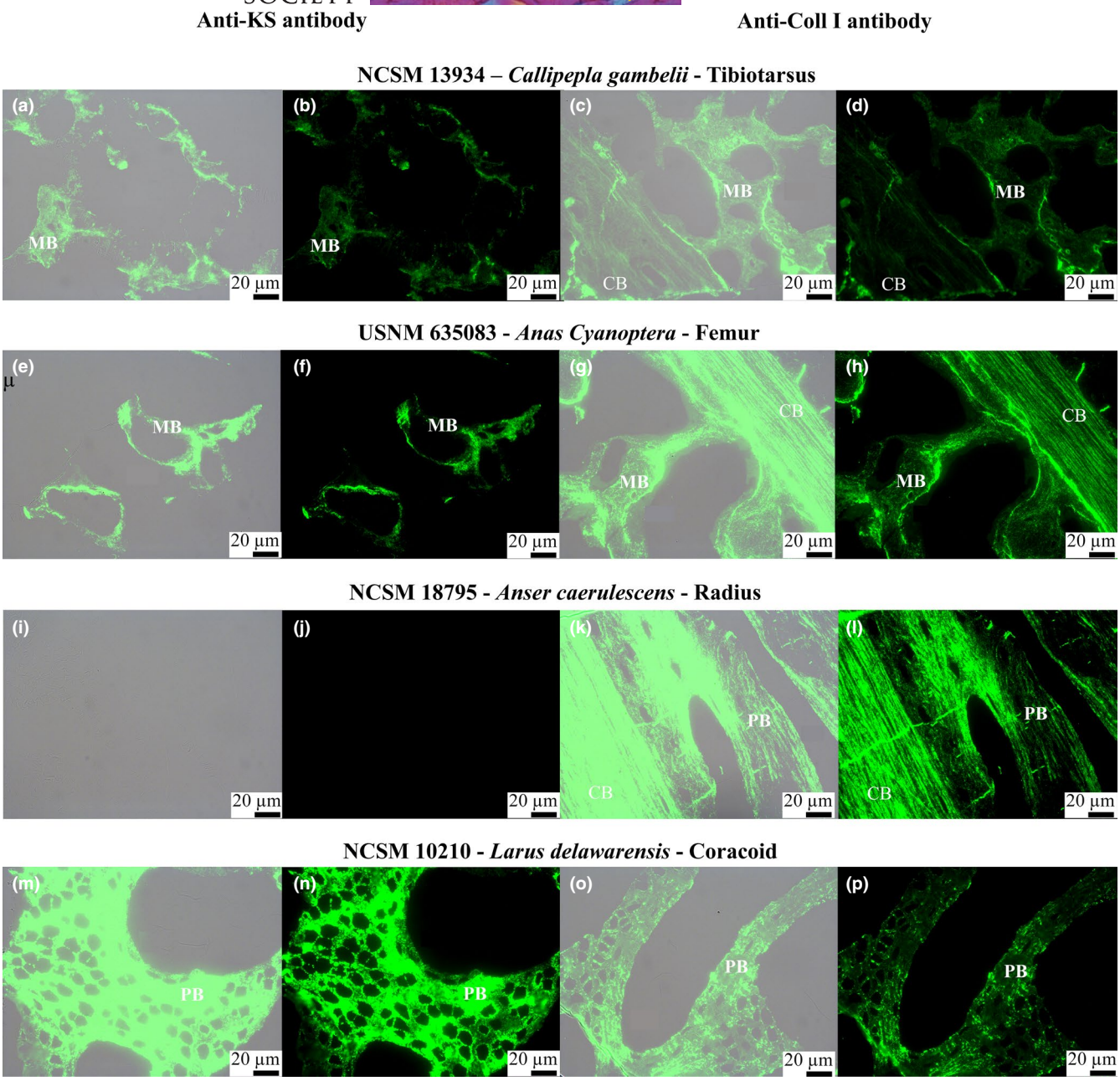

FIGURE 3 Immunochemical staining of bone using monoclonal antibodies raised against the sulfated glycosaminoglycan keratan sulfate (a, b, e, f, i, j, m, and n) or antibodies raised against collagen I (c, d, g, h, k, l, o, and p). Overlay images showing tissue and localized binding (a, c, e, g, i, k, m, and o); Fluorescent images using FITC label (b, d, f, h, j, l, n, and p). Abbreviations: CB, cortical bone tissue; MB, medullary bone; PB, pathological bone tissue

and eosin staining (see Figure 2m-o), chemical differences between these matrices were obvious. Finally, the cartilaginous nodules appeared amorphous under polarized light in petrographic sections, unlike the surrounding bone tissues that exhibit at least some degree of anisotropy (Figure S20c,e).

For immunochemical analyses (immunofluorescence, immunogold labeling), we sampled regions of pathologies that lacked cartilage. Periosteal secondary cartilage has been described as containing both type II collagen (present in other cartilage types) and type I collagen, which dominates in bone (as chondroid bone; Hall, 2005; but also see

FIGURE 4 Immunogold labeling observed under TEM for two selected specimens, NCSM 13934 *Callipepla gambelii* tibiotarsus (a-f) and USNM 635083 *Anas cyanoptera* femur (g-l), containing cortical bone (a-c and g-i) and medullary bone (d-f and j-l). Note that in both specimens, no nanogold particles were seen to specifically bind to the cortical bone tissue, but the medullary bone tissues exhibit numerous nanogold particles (white spheres clearly visible on f, k, and l), testifying of the presence of keratan sulfate

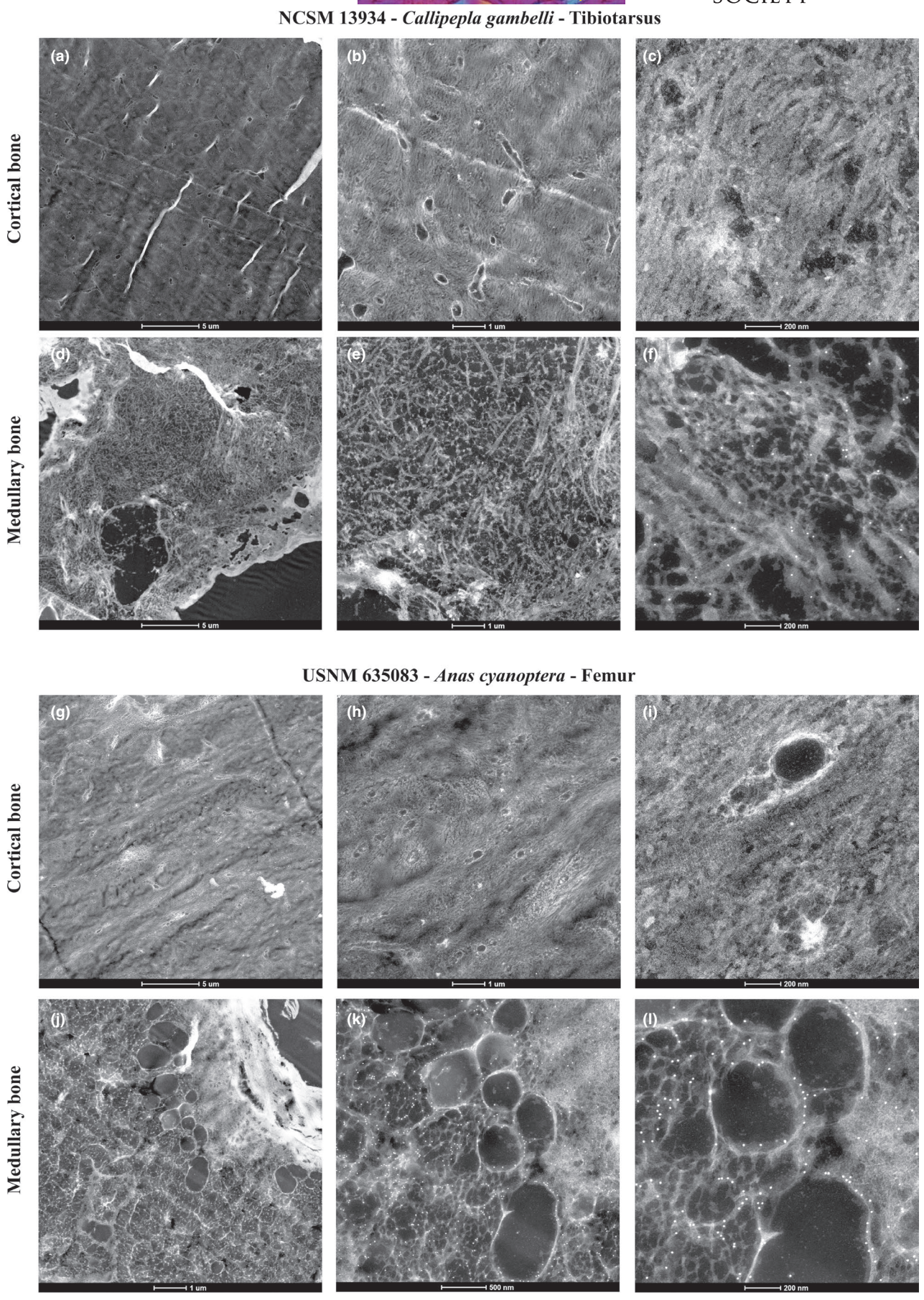
NCSM 13934 - Callipepla gambelli - Tibiotarsus
Cortical bone
Medullary bone
(a)
(b)
(c)
(d)
(e)
(f)
5 um
1 um
200 nm
5 um
1 um
200 nm
USNM 635083 - Anas cyanoptera - Femur
Cortical bone
Medullary bone
(g)
(h)
(i)
(j)
(k)
(l)
5 um
1 um
200 nm
1 um
500 nm
200 nm

Page et al., 1986 who show absence of type I collagen in unstable fracture cartilage). Periosteal secondary cartilage, like medullary bone, also contains keratan sulfate (e.g., Page & Ashhurst, 1987). Sampling such cartilaginous tissues would have introduced false positives in our data (see materials and methods for protocols to ensure samples lacked cartilage).

In our sample of skeletal pathologies, we identified at least nine as fracture calluses (see Table S1), representing different types and stages of healing. Some lacked visible secondary cartilage, while others exhibited cartilaginous nodules. It has been shown that the amount of parallel-fibered/lamellar bone increases as the calluses mature (Glimcher et al., 1980; Shapiro & Wu, 2019). Based upon this criterion, some fracture calluses in our samples are in a more advanced stages of development or remodeling than others, possessing lamellar bone around trabecular cores made of woven and chondroid bone, and bearing secondary osteons.

3.2.2 | Histochemical staining

Identical staining protocols were applied to all 20 sampled pathologies (except the osteopetrotic specimen, for which such analyses has already been undertaken by Schweitzer et al., 2016). In 16 cases, although staining is less strong than for medullary bone specimens, the reactive periosteal and endosteal tissues stained positively with HID and Alcian blue, unlike the surrounding cortical and trabecular bone (Figure 2). Within these pathologies, staining was usually stronger in the matrix patches of chondroid bone exhibiting high concentrations of chondrocyte-like cell lacunae than in the surrounding woven bone (Figure 2k,l). The nodules of cartilage were also more strongly stained than the surrounding pathological woven bone and chondroid bone tissues (Figure 2m-o). Four specimens, including the ulna of NCSM 5802 *Cygnus columbianus* and the tibiotarsus of NCSM 23657 *Gavia immer*, did not show staining with these histochemical stains. In both cases, these pathologies correspond to old fracture calluses that have undergone significant remodeling (Figure S20g,h).

3.2.3 | Immunofluorescence

Some of the pathological specimens tested were negative for binding to anti-keratan sulfate antibodies on both the reactive endosteal and normal cortical bone tissues (Table S2). This is the case, for example, of the fracture callus of specimen NCSM 18795 *Anser caerulescens* (Figure 3i,j). Antibodies to type I collagen were positive for binding on both the cortical and adjacent endosteal reactive bone tissues (Figure 3k,l). However, other specimens with endosteal reactive tissues showed strong positive binding with both anti-keratan sulfate (Figure 3m,n) and anti-type I collagen (Figure 3o,p) antibodies.

3.2.4 | Ultrastructural observations (with TEM) and immunogold labeling

Five pathological specimens were submitted to in situ analyses on ultrathin sections for greater resolution (Table S2). When tested, the cortical bone tissues associated with pathologies did not show any binding with anti-keratan sulfate antibodies. Endosteal reactive tissues exhibited different ultrastructures, depending on the type of pathology (see Figure 5d-i). Some specimens, such as the radius of NCSM 18795, *A. caerulescens*, did not show any binding to the anti-keratan sulfate antibodies (Figure 5d-i). These results are in agreement with those of immunofluorescence analyses conducted on the same specimen. However, the endosteal pathological tissue of NCSM 10210, *L. delawarensis* showed a spongiose ultrastructure, reminiscent of the medullary bone matrix, and strong and specific binding (Figure 5g-i); results also congruent with immunofluorescence analyses on this specimen. Finally, the osteopetrotic sample did not exhibit any binding, supporting results obtained from previous immunofluorescence analyses conducted by Schweitzer et al. (2016).

4 | DISCUSSION

4.1 | Keratan sulfate as a marker for MB

In modern birds, keratan sulfate has long been recognized as a marker of medullary bone, because under normal deposition, the matrix of structural bone (cortical and trabecular) does not contain this specific glycosaminoglycan. Our results confirm that medullary bone matrix strongly reacts with Alcian blue and HID, unlike the associated cortical and trabecular bone (encompassing woven to lamellar bone tissues, regardless of whether they are periosteal or endosteal in origin). This positive staining results from the different chemical compositions of these tissues; medullary bone containing more abundant and different glycosaminoglycans when compared to the surrounding structural bone (Bonucci & Gherardi, 1975; Candlish & Holt, 1971; Yamamoto et al., 2005). Our analyses also demonstrate that anti-keratan sulfate antibodies abundantly bind to medullary bone matrix in both immunofluorescent and immunogold studies, testifying that medullary bone matrix contains keratan sulfate in high concentrations. Our results thereby confirm that, in modern birds, keratan sulfate is a reliable marker of medullary bone.

However, our data also reveal that most pathological reactive tissues (either periosteal or endosteal) also stain with Alcian blue and HID, albeit to a lesser extent. This indicates that most sampled pathologies contained detectable amounts of glycosaminoglycans and moreover, that these histochemical staining methods are not adequate to discriminate between medullary bone and structurally similar, endosteally-derived pathological tissues. In fact, chemical staining protocols with Alcian blue and HID used in this study are standard methodologies for localizing high concentrations of glycosaminoglycans in the matrix of cartilage and bone tissues of extant vertebrates (Bailleul et al., 2020; Canoville et al., 2019, 2020a; Page & Ashhurst, 1987; Sobue & Takeuchi, 1979; Yamamoto et al., 2005). There are no chemical staining methods that are sufficiently specific to differentiate between glycosaminoglycans (Page & Ashhurst, 1987); both dyes (HID and Alcian blue) will detect sulfated (e.g.,

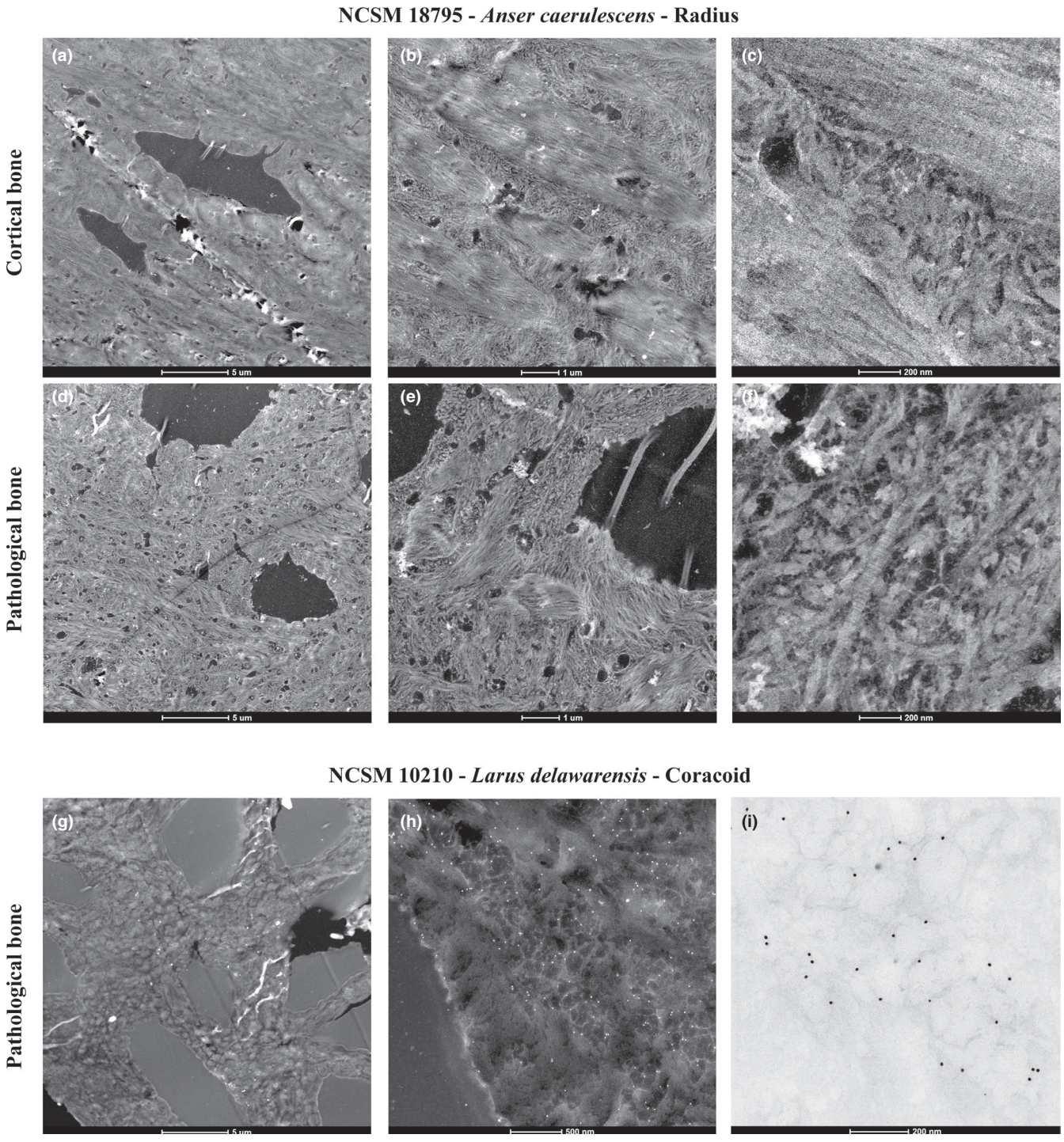

FIGURE 5 Immunogold labeling observed under TEM for two selected specimens, NCSM 18795 *Anser caerulescens* radius (a-f) and NCSM 10210 *Larus delawarensis* coracoid (g-i), containing cortical bone (a-c) and endosteal pathological tissues (d-f and g-i). Note that in NCSM 18795 *A. caerulescens* radius, no nanogold particles were seen to specifically bind to the cortical or endosteal pathological tissues. Numerous nanogold particles were seen to specifically bind to the endosteal pathological tissue of NCSM 10210 *L. delawarensis* coracoid (spheres clearly visible in h and i), testifying of the presence of keratan sulfate in this specimen

keratan sulfate) and non-sulfated carboxylated (e.g., hyaluronic acid) glycosaminoglycans (Page & Ashhurst, 1987; Schumacher & Adam, 1994).

Immunological analyses using the specific monoclonal antibody anti-keratan sulfate are more specific than chemical staining and have thus been used complementarily and in tandem to screen specifically for the presence of keratan sulfate (Page & Ashhurst, 1987; Schumacher & Adam, 1994; Schweitzer et al., 2016; Yamamoto et al., 2005). Therefore, to test whether histochemical staining we observe in our skeletal pathologies was due, at least in part, to the presence of the glycosaminoglycan keratan sulfate, we submitted a subsample of our specimens to immunochemical analyses (with

immunofluorescence and immunogold) using monoclonal anti-keratan sulfate antibodies. When present, secondary periosteal cartilage, reported to contain keratan sulfate by previous authors (Hall, 2005), was carefully excluded from our analyses. We found that, whereas some samples did not react with the anti-keratan sulfate antibodies, others contained significant amounts of keratan sulfate (Table S2), including the pathological reactive tissues seen in the coracoid of NCSM 10210 *L. delawarensis* and the femur of NCSM 19884 *Larus argentatus*. As in several sampled pathologies, the reactive endosteal and periosteal tissues are mostly composed of a highly vascularized and trabecular scaffold. The cores of these trabeculae contain a tissue belonging to the chondroid bone spectrum and can be associated, to some extent, with woven bone directly deposited on to it (Prondvai et al., 2020; Witten et al., 2010). Our results indicate that although the histochemical stains and immunological analyses used here are reliable indicators for the presence of keratan sulfate, they cannot be used in isolation to discriminate between medullary bone and some endosteal pathological tissues (particularly those containing chondroid bone) in avian or non-avian dinosaurs, because both tissue types can contain keratan sulfate.

4.2 | The problem of chondroid bone

The microstructure and chemistry of bone pathologies and fracture repairs (i.e., calluses) have been extensively studied. Although often misidentified, and probably underreported (see review by Beresford, 1981), chondroid bone has been shown to be a major constituent of skeletal pathologies (e.g., tumors, sarcomas) and developing fracture calluses in mammals, birds and other vertebrates (Beresford, 1981; Franch et al., 1998; Hall & Witten, 2018; Nyssen-Behets et al., 1988). This tissue forms rapidly (Franch et al., 1998; Hall, 2015; Prondvai et al., 2020) and thus, in the case of bone repair, ensures a rapid healing process. Previous studies have described the formation of fracture calluses in different mammalian species and showed that woven bone appeared as the *second* tissue in the fracture repair, depositing on a pre-existing framework of either chondroid bone (endosteally and periosteally) or calcified cartilage (Franch et al., 1998; Nyssen-Behets et al., 1988).

The characteristic chondroid bone pattern of highly calcified and fibrous matrix surrounding numerous irregular, large, and confluent cell lacunae (Franch et al., 1998; Witten et al., 2010) shares microstructural features with woven bone (Dhem et al., 1989; Goret-Nicaise & Dhem, 1985; Marotti, 2010), and we suspect that these tissues are often conflated. For example, in their reviews of woven bone and static osteogenesis, Marotti (2010) and Shapiro and Wu (2019) mention that in the process of fracture healing, the first periosteal and endosteal deposits on the original cortical bone are comprised of rapidly deposited woven bone. Similarly, Glimcher et al., 1980 studied the different stages of healing in a chicken fracture callus and noted initial formation of a woven bone trabecular meshwork. However, in the case of fracture healing, this trabecular meshwork should be partly composed of chondroid bone tissue (Beresford, 1981; Franch et al., 1998; Nyssen-Behets et al., 1988).

Page and Ashhurst (1987) also investigated the process of fracture healing in rabbit tibiae and described the initial deposition of cancellous bone for the formation of the callus, without specifying the nature of its matrix. They further added that in this bone tissue, osteocyte lacunae are seen as spaces, but are not further differentiated. This description suggests that the cell lacunae they observed did not show any characteristic features, such as canaliculi. Their figures 7 and 8 illustrate a few trabeculae of this cancellous bone and show high concentration of cell lacunae that lack clear canaliculi and vary in size and orientation. This bone tissue is thus reminiscent of the chondroid bone observed in most of our pathological samples. Moreover, Page and Ashhurst (1987) used similar histochemical tests (Alcian Blue and HID staining, immunochemistry with anti-keratan sulfate antibodies) to decipher the amounts and types of glycosaminoglycans in the different tissues constituting the fracture callus. As found in our sample, their data showed differences in dye and antibodies-binding between the different-aged fractures calluses (few days to few weeks) and variation within the cancellous bone matrices. Indeed, they found that in some developing fracture calluses, the cancellous bone matrix strongly stained with Alcian blue and HID. The 5-D-4 antibodies also bound to most of the matrix of the newly formed trabeculae, revealing the presence of keratan sulfate in this tissue. As the trabeculae mature, staining and binding became restricted to the core of the trabeculae and the matrix around the cell lacunae, respectively. That could be explained by the fact that the central regions of trabeculae are mostly formed by chondroid bone, whereas the peripheral regions are lined by true woven bone, as described by Nyssen-Behets et al. (1988) and Franch et al. (1998) and observed in some of our samples (Figure 2, Figure S20i,j).

The results of Page and Ashhurst (1987) are congruent with our data and first support that keratan sulfate is present in the trabecular bone tissue of some fracture calluses, depending on the stage of healing. Dunham et al. (1983) also reported on the presence of keratan sulfate in the bone of healing rat fractures. Second, Page and Ashhurst's (1987) observations of variable staining and binding depending on the degree of maturation of the callus could explain why some of our specimens did not stain with Alcian blue and HID or bind to the 5-D-4 antibodies. This is the case, for example, of NCSM 5802 *C. columbianus* and NCSM 23657 *G. immer* that could simply represent calluses in which most of the initial chondroid tissue has been remodeled. Histological observations of these specimens confirm that these fracture calluses mostly consist of parallel-fibered bone and secondary osteons (Figures S14 and S20g,h).

Interestingly, medullary bone has been considered a type of chondroid bone (Beresford, 1981), which further highlights the problem of discriminating medullary bone from some endosteal pathologies. Medullary bone and some types of chondroid bone share features in common (Beresford, 1981), other than the fact that they can have an endosteal origin and be synthesized de novo, without a cartilaginous template. The features that place these tissues on a continuum between cartilage and bone include their

higher concentration of proteoglycans in the matrix (including sometimes keratan sulfate; Wang et al., 2005; the present study), their high degree of mineralization (Franch et al., 1998; Goret-Nicaise & Dhem, 1985), and the relative abundance of large cellular lacunae relative to other bone tissues (see Beresford, 1981: Table S1 and reference therein; Harrison & Clark, 1986). Medullary bone (at least in neornithes; see Canoville et al., 2020a) and some chondroid bone also share a trabecular organization, with a woven-fibered matrix that looks similar at the nanoscale (see for example Figures 4k and 5h). These common microstructural and chemical features are likely linked to the fact that these tissues are "short-lived" and form via high rates of osteogenesis (Beresford, 1981; Dacke et al., 1993; Hall, 2015; Knott & Bailey, 1999; Prondvai et al., 2020). For example, chondroid bone is common in normal embryonic and pathological bone growth (Beresford, 1981), occurring mostly in areas subject to rapid remodeling and reshaping. Prondvai et al (2020) reported the presence of periosteal chondroid bone in the limb bone shaft development of fast growing ducklings (from post hatching to 30 days of age) where one would rather expect woven bone tissue, based on commonly accepted principles of diametrical long bone growth in amniotes (see for example Marotti, 2010; Shapiro & Wu, 2019). Medullary bone is also known for its ephemeral nature associated with fast deposition and subsequent resorption rates during lay (Dacke et al., 1993; Kerschnitzki et al., 2014).

To date, chondroid bone, which remains overlooked in extant vertebrates, has only been reported in skull bones of embryonic and hatchling hadrosaurs (Bailleul et al., 2016). To our knowledge, this tissue has never been recognized in fossil skeletal pathologies, although histological descriptions of non-avian dinosaur pathologies are common (e.g., Chinsamy et al., 2016; Chinsamy & Tumarkin-Deratzian, 2009; García et al., 2017; Redelstorff et al., 2015; Straight et al., 2009; Tschopp et al., 2016). It is important to note that, in some cases, the stage of healing might be too advanced to see chondroid tissue. However, some authors reported the presence of high concentration of osteocyte lacunae that lack canaliculi in paleopathologies (Cerda et al., 2014; Redelstorff et al., 2015). Recently, Straight et al. (2009) described hadrosaur bone lesions, which were recognized histologically. These authors noted that in one non-remodeled fracture callus, bone trabeculae presented clusters of densely packed and randomly oriented cell lacunae, reminiscent of chondrocytes and orders of magnitude larger than those of typical osteocytes. Based upon these features, some of these tissues could be chondroid bone, although they were not specifically identified as such.

Future studies may determine whether there are definite qualitative or quantitative chemical or microstructural differences between medullary bone and reactive chondroid bone. Although both medullary bone and chondroid bone present numerous osteocytes (lacunae), the morphology and size of the latter may differ. For example, Beresford (1981: Table S1) noted that medullary bone osteocytes present processes (i.e., filipodia), whereas chondroid bone cells do not (see also Witten et al., 2010). However, other authors noted the presence of short cellular processes in some chondroid bone cells (e.g., Prondvai et al., 2020).

4.3 | Implications for sex determination in extinct archosaurs

Several researchers have reflected on a set of criteria to confidently identify medullary bone and distinguish this reproductive tissue from other bone tissue types in the fossil record (see Chinsamy et al., 2016; O'Connor et al., 2018 and the recent review in Canoville et al., 2020a). However, the confident identification of this tissue in fossil specimens remains problematic. The development of definitive morphological criteria for medullary bone in extinct species is complicated by the structural variation observed within living birds (Canoville et al., 2020a; O'Connor et al., 2018), the possibility that the morphology of medullary bone varied during its early evolution (Canoville et al., 2020a) and may not be consistent with what is observed in extant birds, and the fact that medullary bone shares microstructural characteristics with certain pathological tissues (Beresford, 1981; the present study). Here we demonstrate similar challenges in medullary bone identification that result from chemical overlap with pathological tissues. In the absence of preservation or treatment biases (a particular problem for fossil materials), our results indicate that the *absence* of keratan sulfate can be used to reject a hypothesis of medullary bone (i.e., all medullary bone contains keratan sulfate) and conversely, that the *presence* of keratan sulfate is inadequate to rule out the alternative hypothesis of pathological origin for potential medullary bone tissues in fossil vertebrates (i.e., keratan sulfate is present in medullary bone and also in some pathological bone, particularly those containing chondroid bone). Confident identifications of medullary bone in fossil vertebrates currently require multiple morphological, developmental, chemical, and location-based (e.g., skeletal distribution patterns, inverse relationships with pneumaticity) criteria to amass a preponderance of evidence (e.g., Canoville et al., 2020a; Chinsamy et al., 2016; O'Connor et al., 2018). No *single* criterion can be used to reject a hypothesis of pathological origin for endosteal tissues in fossil vertebrates.

ACKNOWLEDGMENTS

The authors thank the different (assistant) curators for facilitating access to their collections and loaning specimens: Brian O'shea and John Gerwin (North Carolina Museum of Natural Sciences, Raleigh, NC); Helen James and Christopher Milensky (National Museum of Natural History, Smithsonian Institution, Washington, DC). We thank Holly Woodward (Oklahoma State University Center for Health Sciences, Tulsa, USA) for providing access to the kiwi specimen. The authors also thank Kyla Beguesse for confirming our fracture callus identifications. Justin Gladman (Shared Materials Instrumentation Facility, Duke University, Durham, NC) is acknowledged for his assistance with micro-CT scanning. Finally, the authors thank the two reviewers, Pavel Skutschas and Anusuya Chinsamy-Turan, for their constructive comments and suggestions that improved our manuscript. Part of this work

(TEM observations) was performed at the Analytical Instrumentation Facility (AIF) at North Carolina State University, which is supported by the State of North Carolina and the National Science Foundation (award number ECCS-1542015). The AIF is a member of the North Carolina Research Triangle Nanotechnology Network (RTNN), a site in the National Nanotechnology Coordinated Infrastructure (NNCI). This research was funded by a National Science Foundation award no. 1552328 to LEZ and MHS.

AUTHOR CONTRIBUTIONS

AC, LEZ, and MHS designed the study. AC and WZ ran the analyses, collected, and analyzed the data. AC, LEZ, and MHS wrote the manuscript. All authors read and approved the final version of the manuscript.

DATA AVAILABILITY STATEMENT

The datasets generated and/or analyzed during the current study are available in the Electronic Supplementary Material documents and in the MorphoSource repository, under the project P1053 at https://www.morphosource.org (Canoville et al., 2020b).

ORCID

Aurore Canoville https://orcid.org/0000-0002-9798-176X
Lindsay E. Zanno https://orcid.org/0000-0002-1654-1990
Wenxia Zheng https://orcid.org/0000-0002-1122-9826
Mary H. Schweitzer https://orcid.org/0000-0002-0427-3829

REFERENCES

Bailleul, A.M., Nyssen-Behets, C., Lengelé, B., Hall, B.K. & Horner, J.R. (2016) Chondroid bone in dinosaur embryos and nestlings (Ornithischia: Hadrosauridae): Insights into the growth of the skull and the evolution of skeletal tissues. *Comptes Rendus Palevol*, 15, 49–64.

Bailleul, A.M., O'Connor, J., Zhang, S., Li, Z., Wang, Q., Lamanna, M.C. et al. (2019) An Early Cretaceous enantiornithine (Aves) preserving an unlaid egg and probable medullary bone. *Nature Communications*, 10, 1275.

Bailleul, A.M., Zheng, W., Horner, J.R., Hall, B.K., Holliday, C.M. & Schweitzer, M.H. (2020) Evidence of proteins, chromosomes and chemical markers of DNA in exceptionally preserved dinosaur cartilage. *National Science Review*, 7(4), 815–822. https://doi.org/10.1093/nsr/nwz206

Banes, A.J. & Smith, R.E. (1977) Biological characterization of avian osteopetrosis. *Infection and Immunity*, 16, 876–884.

Barden, H.E. & Maidment, S.C. (2011) Evidence for sexual dimorphism in the stegosaurian dinosaur *Kentrosaurus aethiopicus* from the Upper Jurassic of Tanzania. *Journal of Vertebrate Paleontology*, 31, 641–651.

Beresford, W.A. (1981) *Chondroid bone, secondary cartilage and metaplasia*. Munich: Urban and Schwarzenberg.

Bonucci, E. & Gherardi, G. (1975) Histochemical and electron microscope investigations on medullary bone. *Cell and Tissue Research*, 163, 81–97.

Candlish, J.K. & Holt, F.J. (1971) The proteoglycans of fowl cortical and medullary bone. *Comparative Biochemistry and Physiology Part B: Comparative Biochemistry*, 40, 283–290.

Canoville, A., Schweitzer, M.H. & Zanno, L.E. (2019) Systemic distribution of medullary bone in the avian skeleton: Ground truthing criteria for the identification of reproductive tissues in extinct Avemetatarsalia. *BMC Evolutionary Biology*, 19, 71.

Canoville, A., Schweitzer, M.H. & Zanno, L. (2020a) Identifying medullary bone in extinct avemetatarsalians: Challenges, implications and perspectives. *Philosophical Transactions of the Royal Society B: Biological Sciences*, 375, 20190133.

Canoville, A., Zanno, L.E., Zheng, W. & Schweitzer, M.H. (2020b) Keratan sulfate as a marker for medullary bone in fossil vertebrates. MorphoSource repository, project no. P1053. Retrieved from https://www.morphosource.org

Cerda, I.A., Chinsamy, A. & Pol, D. (2014) Unusual endosteally formed bone tissue in a Patagonian basal sauropodomorph dinosaur. *The Anatomical Record*, 297, 1385–1391.

Cerda, I.A. & Pol, D. (2013) Evidence for gender-specific reproductive tissue in a basal sauropodomorph dinosaur from the Late Triassic of Argentina. *Ameghiniana*, 50, 11–12R.

Chapman, R.E., Weishampel, D.B., Hunt, G. & Rasskin-Gutman, D. (1997) Sexual dimorphism in dinosaurs. In D.L. Wolberg, E. Stump, & G.S. Rosenberg (Eds). *Dinofest international, proceedings of a symposium sponsored by Arizona State University* (pp. 83–93). Philadelphia, PA: Philadelphia Academy of Natural Sciences.

Chinsamy, A., Cerda, I. & Powell, J. (2016) Vascularised endosteal bone tissue in armoured sauropod dinosaurs. *Scientific Reports*, 6, 24858.

Chinsamy, A. & Tumarkin-Deratzian, A. (2009) Pathologic bone tissues in a turkey vulture and a nonavian dinosaur: Implications for interpreting endosteal bone and radial fibrolamellar bone in fossil dinosaurs. *The Anatomical Record*, 292, 1478–1484.

Dacke, C.G., Arkle, S., Cook, D.J., Wormstone, I.M., Jones, S., Zaidi, M. & et al. (1993) Medullary bone and avian calcium regulation. *The Journal of Experimental Biology*, 184, 63–88.

Dhem, A., Goret-Nicaise, M., Dambrain, R., Nyssen-Behets, C., Lengelé, B. & Manzanares, M.C. (1989) Skeletal growth and chondroid tissue. *Italian Journal of Anatomy and Embryology*, 94, 237–241.

Dunham, J., Catterall, A., Bitensky, L. & Chayen, J. (1983) Metabolic changes in the cells of the callus during fracture healing in the rat. *Calcified Tissue International*, 35, 56–61.

Erickson, G.M., Lappin, A.K. & Larson, P. (2005) Androgynous rex–The utility of chevrons for determining the sex of crocodilians and non-avian dinosaurs. *Zoology*, 108, 277–286.

Fang, J. & Hall, B.K. (1997) Chondrogenic cell differentiation from membrane bone periostea. *Anatomy and Embryology*, 196, 349–362.

Fisher, L.W. & Schraer, H. (1982) Keratan sulfate proteoglycan isolated from the estrogen-induced medullary bone in Japanese quail. *Comparative Biochemistry and Physiology Part A: Molecular & Integrative Physiology*, 72, 227–232.

Franch, J., García, F., Camón, J. & Manzanare, M.C. (1998) Backscattered electron imaging of the calcified tissues present in bone healing. *Veterinary and Comparative Orthopaedics and Traumatology*, 11, 105–111.

Francillon-Vieillot, H., de Buffrénil, V., Castanet, J., Géraudie, J., Meunier, F.J., Sire, J.Y. et al. (1990) Microstructure and mineralization of vertebrate skeletal tissues. *Skeletal biomineralization: Patterns, processes and evolutionary trends* (pp. 471–530).

García, R.A., Cerda, I.A., Heller, M., Rothschild, B.M. & Zurriaguz, V. (2017) The first evidence of osteomyelitis in a sauropod dinosaur. *Lethaia*, 50, 227–236.

Glimcher, M.J., Shapiro, F., Ellis, R.D. & Eyre, D.R. (1980) Changes in tissue morphology and collagen composition during the repair of cortical bone in the adult chicken. *The Journal of Bone & Joint Surgery*, 62, 964–973.

Goret-Nicaise, M. (1984) Identification of collagen type I and type II in chondroid tissue. *Calcified Tissue International*, 36, 682–689.

Goret-Nicaise, M. & Dhem, A. (1985) Comparison of the calcium content of different tissues present in the human mandible. *Cells Tissues Organs*, 124, 167–172.

Goret-Nicaise, M. & Dhem, A. (1987) Electron microscopic study of chondroid tissue in the cat mandible. *Calcified Tissue International*, 40, 219–223.

Hadley, J.A., Horvat-Gordon, M., Kim, W.-K., Praul, C.A., Burns, D. & Leach, R.M. Jr (2016) Bone sialoprotein keratan sulfate proteoglycan (BSP-KSPG) and FGF-23 are important physiological components of medullary bone. *Comparative Biochemistry and Physiology Part A: Molecular & Integrative Physiology*, 194, 1–7.

Hall, B.K. (2005) *Bones and cartilage: Developmental and evolutionary skeletal biology*. Elsevier Academic Press.

Hall, B.K. (2015) Vertebrate skeletal tissues. *BK Hall, Bones and cartilage* (pp. 3–16).

Hall, B.K. & Witten, P.E. (2018) Plasticity and variation of skeletal cells and tissues and the evolutionary development of actinopterygian fishes. *Evolution and development of fishes*.

Harrison, J.R. & Clark, N.B. (1986) Avian medullary bone in organ culture: Effects of vitamin D metabolites on collagen synthesis. *Calcified Tissue International*, 39, 35–43.

Hübner, T.R. (2012) Bone histology in *Dysalotosaurus lettowvorbecki* (Ornithischia: Iguanodontia) – Variation, growth, and implications. *PLoS One*, 7, e29958.

Jin, X., Varricchio, D.J., Poust, A.W. & He, T. (2020) An oviraptorosaur adult-egg association from the Cretaceous of Jiangxi Province, China. *Journal of Vertebrate Paleontology*, e1739060.

Kerschnitzki, M., Zander, T., Zaslansky, P., Fratzl, P., Shahar, R. & Wagermaier, W. (2014) Rapid alterations of avian medullary bone material during the daily egg-laying cycle. *Bone*, 69, 109–117.

Knott, L. & Bailey, A.J. (1999) Collagen biochemistry of avian bone: Comparison of bone type and skeletal site. *British Poultry Science*, 40, 371–379.

Lamm, E.T. (2013) Preparation and sectioning of specimens. *Bone histology of fossil tetrapods: Advancing methods, analysis, and interpretation* (pp. 55–160).

Lee, A.H. & Werning, S. (2008) Sexual maturity in growing dinosaurs does not fit reptilian growth models. *Proceedings of the National Academy of Sciences of the United States of America*, 105, 582–587.

Mallon, J.C. (2017) Recognizing sexual dimorphism in the fossil record: Lessons from nonavian dinosaurs. *Paleobiology*, 43, 495–507.

Marotti, G. (2010) Static and dynamic osteogenesis. *Italian Journal of Anatomy and Embryology*, 115, 123–126.

Mitchell, J., Legendre, L.J., Lefèvre, C. & Cubo, J. (2017) Bone histological correlates of soaring and high-frequency flapping flight in the furculae of birds. *Zoology*, 122, 90–99.

Nyssen-Behets, C., Dhem, A., Vandersmissen, A. & Ansay, M. (1988) Spontaneous fracture in bovine fluorosis: Microradiographic aspects. A case report. *Annales de Radiologie*, 31, 451–454.

O'Connor, J., Erickson, G.M., Norell, M., Bailleul, A.M., Hu, H. & Zhou, Z. (2018) Medullary bone in an Early Cretaceous enantiornithine bird and discussion regarding its identification in fossils. *Nature Communications*, 9.

Padian, K. & Horner, J.R. (2011) The evolution of "bizarre structures" in dinosaurs: Biomechanics, sexual selection, social selection or species recognition? *Journal of Zoology*, 283, 3–17.

Padian, K. & Horner, J.R. (2014) The species recognition hypothesis explains exaggerated structures in non-avialan dinosaurs better than sexual selection does. *Comptes Rendus Palevol*, 13, 97–107.

Page, M., Hogg, J. & Ashhurst, D.E. (1986) The effects of mechanical stability on the macromolecules of the connective tissue matrices produced during fracture healing. *I. The collagens. The Histochemical Journal* 18, 251–265.

Page, M. & Ashhurst, D.E. (1987) The effects of mechanical stability on the macromolecules of the connective tissue matrices produced during fracture healing. II. The glycosaminoglycans. *The Histochemical Journal*, 19, 39–61.

Persons, W.S.P. IV, Funston, G.F., Currie, P.J. & Norell, M.A. (2015) A possible instance of sexual dimorphism in the tails of two oviraptorosaur dinosaurs. *Scientific Reports*, 5.

Prondvai, E. (2017) Medullary bone in fossils: Function, evolution and significance in growth curve reconstructions of extinct vertebrates. *Journal of Evolutionary Biology*, 30, 440–460.

Prondvai, E., Witten, P.E., Abourachid, A., Huysseune, A. & Adriaens, D. (2020) Extensive chondroid bone in juvenile duck limbs hints at accelerated growth mechanism in avian skeletogenesis. *Journal of Anatomy*, 236, 463–473.

Prum, R.O., Berv, J.S., Dornburg, A., Field, D.J., Townsend, J.P., Lemmon, E.M. & et al. (2015) A comprehensive phylogeny of birds (Aves) using targeted next-generation DNA sequencing. *Nature*, 526, 569–573.

Redelstorff, R., Hayashi, S., Rothschild, B.M. & Chinsamy, A. (2015) Non-traumatic bone infection in stegosaurs from Como Bluff, Wyoming. *Lethaia*, 48, 47–55.

Saitta, E.T. (2015) Evidence for sexual dimorphism in the plated dinosaur *Stegosaurus mjosi* (Ornithischia, Stegosauria) from the Morrison Formation (Upper Jurassic) of Western USA. *PLoS One*, 10, e0123503.

Sato, T., Cheng, Y.N., Wu, X.C., Zelenitsky, D.K. & Hsiao, Y.F. (2005) A pair of shelled eggs inside a female dinosaur. *Science*, 308, 375.

Schumacher, U. & Adam, E. (1994) Standardization of staining in glycosaminoglycan histochemistry: Alcian blue, its analogues, and diamine methods. *Biotechnic & Histochemistry*, 69, 18–24.

Schweitzer, M.H., Wittmeyer, J.L. & Horner, J.R. (2005) Gender-specific reproductive tissue in ratites and *Tyrannosaurus rex*. *Science*, 308, 1456–1460.

Schweitzer, M.H., Zheng, W., Zanno, L., Werning, S. & Sugiyama, T. (2016) Chemistry supports the identification of gender-specific reproductive tissue in *Tyrannosaurus rex*. *Scientific Reports*, 6, 23099.

Shapiro, F. & Wu, J. (2019) Woven bone overview: Structural classification based on its integral role in developmental, repair and pathological bone formation throughout vertebrate groups. *European Cells and Materials*, 38, 137–167.

Simkiss, K. (1961) Calcium metabolism and avian reproduction. *Biological Reviews*, 36, 321–359.

Skutschas, P.P., Boitsova, E.A., Averianov, A.O. & Sues, H.-D. (2017) Ontogenetic changes in long-bone histology of an ornithomimid theropod dinosaur from the Upper Cretaceous Bissekty Formation of Uzbekistan. *Historical Biology*, 29, 715–729.

Sobue, M. & Takeuchi, J. (1979) Chondroitinase-resistant sulfated glycosaminoglycans synthesized by cartilages of chick embryos and of newborn chickens and rats. *Calcified Tissue International*, 27, 269–273.

Spicer, S.S. (1965) Diamine methods for differentiating mucosubstances histochemically. *Journal of Histochemistry & Cytochemistry*, 13, 211–234.

Straight, W.H., Davis, G.L., Skinner, H.C.W., Haims, A., McClennan, B.L. & Tanke, D.H. (2009) Bone lesions in hadrosaurs: Computed tomographic imaging as a guide for paleohistologic and stable-isotopic analysis. *Journal of Vertebrate Paleontology*, 29, 315–325.

Street, J., Bao, M., deGuzman, L., Bunting, S., Peale, F.V. Jr, Ferrara, N. et al. (2002) Vascular endothelial growth factor stimulates bone repair by promoting angiogenesis and bone turnover. *Proceedings of the National Academy of Sciences of the United States of America*, 99, 9656–9661.

Tschopp, E., Wings, O., Frauenfelder, T. & Rothschild, B. (2016) Pathological phalanges in a camarasaurid sauropod dinosaur and implications on behaviour. *Acta Palaeontologica Polonica*, 61, 125–134.

Varricchio, D.J., Moore, J.R., Erickson, G.M., Norell, M.A., Jackson, F.D. & Borkowski, J.J. (2008) Avian paternal care had dinosaur origin. *Science*, 322, 1826–1828.

Wang, X., Ford, B.C., Praul, C.A. & Leach, R.M. Jr (2005) Characterization of the non-collagenous proteins in avian cortical and medullary bone. *Comparative Biochemistry and Physiology Part B: Biochemistry and Molecular Biology*, 140, 665–672.

Werning, S. (2018) Medullary bone is phylogenetically widespread and its skeletal distribution varies by taxon. *Journal of Ornithology*, 159, 527–543.

Witten, P.E., Huysseune, A. & Hall, B.K. (2010) A practical approach for the identification of the many cartilaginous tissues in teleost fish. *Journal of Applied Ichthyology*, 26, 257–262.

Woodward, H.N., Freedman Fowler, E.A., Farlow, J.O. & Horner, J.R. (2015) *Maiasaura*, a model organism for extinct vertebrate population biology: A large sample statistical assessment of growth dynamics and survivorship. *Paleobiology*, 41, 503–527.

Yamamoto, T., Nagaoka, N., Hirata, A., Nakamura, H., Inoue, M., Kawai, M. & et al. (2005) Ultrastructural and immunohistochemical studies of medullary bone calcification, with special reference to sulphated glycosaminoglycans. *Journal of Electron Microscopy*, 54, 29–34.

Yamamoto, T., Nakamura, H., Tsuji, T. & Hirata, A. (2001) Ultracytochemical study of medullary bone calcification in estrogen injected male Japanese quail. *The Anatomical Record*, 264, 25–31.

Zheng, X., O'Connor, J., Huchzermeyer, F., Wang, X., Wang, Y., Wang, M. & et al. (2013) Preservation of ovarian follicles reveals early evolution of avian reproductive behaviour. *Nature*, 495, 507–511.

SUPPORTING INFORMATION

Additional supporting information may be found online in the Supporting Information section.

How to cite this article: Canoville A, Zanno LE, Zheng W, Schweitzer MH. Keratan sulfate as a marker for medullary bone in fossil vertebrates. *J Anat*. 2020;00:1–16. https://doi.org/10.1111/joa.13388